ARCTIC ECOLOGY

Arctic sea ice retreat fuels boreal forest advance

Roman J. Dial[1]*, Colin T. Maher[2]†, Rebecca E. Hewitt[3]‡, Amy M. Wockenfuss[1]§, Russell E. Wong[1], Daniel J. Crawford[2], Madeline G. Zietlow[1]¶, Patrick F. Sullivan[2]

Climate-induced northward advance of boreal forest is expected to lessen albedo, alter carbon stocks, and replace tundra, but where and when this advance will occur remains largely unknown. Using data from 19 sites across 22 degrees of longitude along the tree line of northern Alaska, we show a stronger temporal correlation of tree ring growth with open water uncovered by retreating Arctic sea ice than with air temperature. Spatially, our results suggest that tree growth, recruitment, and range expansion are causally linked to open water through associated warmer temperatures, deeper snowpacks, and improved nutrient availability. We apply a meta-analysis to 82 circumarctic sites, finding that proportionally more tree lines have advanced where proximal to ongoing sea ice loss. Taken together, these findings underpin how and where changing sea ice conditions facilitate high-latitude forest advance.

Alexander von Humboldt was the first to identify temperature as the primary determinant of tree line (*1*)—the (often abrupt) separation of forests and woodlands from shorter statured shrubs and herbaceous vegetation on mountains and at high latitudes. Supported by evidence that forests expanded during interglacial periods (*2*–*6*), Humboldt's idea now prompts an expectation of an impending boreal forest shift. Replacement of tundra by forest would lower albedo (*6*, *7*), release carbon from soils (*6*, *7*), and increase landscape flammability (*2*, *5*, *6*, *8*), all of which could amplify warming (*6*, *7*). However, rising temperatures alone cannot shift forest-tundra boundaries (ecotones) (*2*–*6*, *8*–*29*). Although some boreal tree species are expanding their geographic ranges at post-Pleistocene rates in Fennoscandia (*9*) and northwest Alaska (*16*), many circumarctic ecotones elsewhere are slow-moving or stagnant (*2*–*6*, *8*–*15*) even where temperatures exceed thresholds thought to determine tree line locations (*30*). Ecotone inertia appears particularly acute in eastern Siberia (*3*, *8*, *27*–*29*) and northern Canada (*2*, *3*, *10*–*15*, *21*).

Because individual trees must pass through several size-related stages to reach sexual maturity (*26*), previous field studies have focused on life-history complexity and nonlinear responses to warming that could explain slow climate-driven ecotone advance. These studies show that cones and catkins often contain few viable seeds (*19*–*21*, *28*) at the tree line, where reproduction is sensitive to warmth and precipitation (*20*, *28*, *31*). Cool air temperatures (*2*–*5*, *13*, *16*–*18*, *24*, *30*), desiccation (*15*, *32*, *33*), and limited soil nitrogen (*34*) also hamper germination and adult growth. By contrast, atmospheric warming facilitates growth directly through greater cell division (*30*) and indirectly through increased decomposition (*35*–*39*), which improves nutrient availability (*35*–*38*). The insulative value of snowpacks provides similar benefits (*22*, *35*–*38*) but snowpacks additionally protect seedlings from wind damage in winter and desiccation during growing season onset (*2*, *16*, *23*, *39*, *40*). Thus, climate forcing that warms the atmosphere and deepens snowpacks may facilitate forest advance.

One such source of climate forcing is the rapidly opening Arctic Ocean, where reduced sea ice cover leads to lower albedo and greater evaporation (*41*–*44*). Because the timing of maximum open water area coincides with seasonal cooling, the decline of autumn sea ice warms the atmosphere and deepens snowpacks nearby through increased local precipitation recycling (*42*). These dynamics motivate the hypothesis that sea ice retreat plays an important role in ecotone advance. We test hypothetical pathways leading from autumn open water in the Arctic Ocean to ecotone dynamics with data collected throughout Alaska's Brooks Range, where arctic and alpine tree lines converge along a sea ice–influenced climatic gradient (Fig. 1A).

By linking field measures of individual white spruce (*Picea glauca*) and environmental variables to forest advance measured through repeat imagery, we find support for the idea that an increasingly open Arctic Ocean leads to improved growth, recruitment, and range expansion. We confront our hypothesis with a meta analysis of published circumarctic studies of ecotone movement and discover that a greater proportion of ecotones have advanced where nearby seas are rapidly gaining open water in autumn or where little autumn ice covered those seas historically. Fewer ecotones have advanced where proximal to historically persistent sea ice.

More open autumn Arctic Ocean water corresponds to more winter precipitation

Causal relationships, global versus synoptic systems, and feedbacks among sea ice loss, air temperature, and snowfall are not fully resolved, an uncertainty exacerbated by sparse precipitation records at high latitudes (*41*–*44*). Even so, continental climatic conditions of colder, drier winters on nearby landmasses generally correspond to extensive sea ice in adjacent marginal seas, whereas more maritime-like conditions of warmer, snowier winters correspond to more open seas. The Brooks Range, proximal to the Beaufort Sea in the east and the Chukchi Sea in the west, provides an opportunity to compare tree line processes subject to differing sea ice conditions across space and over time.

During October, Arctic Ocean sea ice is at a near minimum and air temperatures are subfreezing (*44*, *45*). Since 1979, satellite monitoring has shown that, on average, October sea ice area covered three-quarters of the Beaufort Sea but only half of the similarly-sized Chukchi Sea (fig. S1A) (*45*). Although Pacific Ocean storm tracks and inflow create more maritime-like Chukchi conditions relative to the Beaufort, ice generally covers both seas January through April (*44*, *45*). As a result of differences in autumn open water, November-March precipitation in Kotzebue on the Chukchi Sea is regularly twice that of Kuparuk on the Beaufort Sea (fig. S1B). When a 30-year (1981 to 2010) climatology [Parameter-Elevation Regressions on Independent Slopes Model (PRISM)] (*46*) is extracted from 22 watersheds at Brooks Range tree lines, the differences in precipitation appear to extend 50 to 350 km inland (fig. S1C). During the PRISM period, Chukchi October sea ice area and Beaufort ice area declined 12,350 $km^2\ y^{-1}$ and 6350 $km^2\ y^{-1}$, respectively.

To investigate the influence of 1979-2017 October open water area (OWA) on ecotones, we sampled biotic and abiotic variables at 81 tree lines arrayed across 19 watersheds. Using sea ice area (*47*), we calculated for each watershed the distance-weighted average exposure to annual October open water area as a time series (OWA series, in $10^5\ km^2$) (fig. S2) that we compared with tree ring widths. Other biotic and abiotic variables that we measured at tree lines were evaluated in the spatial context of overall mean values of the OWA series ($\overline{OWA}$). In addition, from repeat imagery, we estimated forest advance over four decades in 22 watersheds and compared those rates with Theil-Sen trends of the OWA series (OWA trend) and to PRISM precipitation. Greater

[1]Institute for Culture and Environment, Alaska Pacific University, Anchorage, AK, USA. [2]Environment and Natural Resources Institute, University of Alaska Anchorage, Anchorage, AK, USA. [3]Center for Ecosystem Science and Society, Northern Arizona University, Flagstaff, AZ, USA.
*Corresponding author. Email: roman@alaskapacific.edu
†Present address: ORISE Fellow, Anchorage Forestry Sciences Laboratory, Pacific Northwest Research Station, USDA Forest Service, Anchorage, AK, USA.
‡Present address: Department of Environmental Science, Amherst College, Amherst, MA, USA. §Present address: Alaska Department of Environmental Conservation, Anchorage, AK, USA.
¶Present address: Environment and Natural Resources Institute, University of Alaska Anchorage, Anchorage, AK, USA.

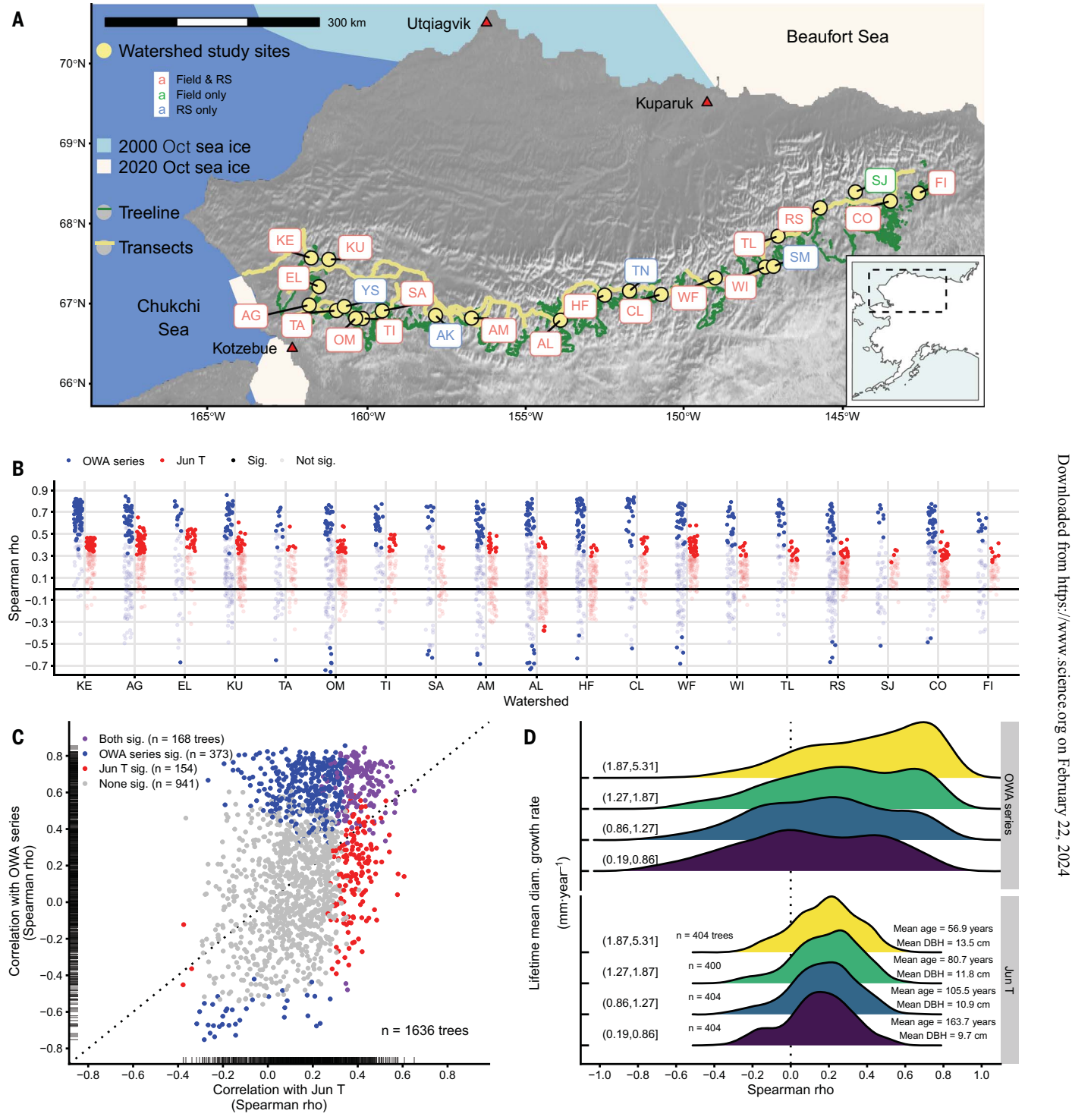

Fig. 1. Radial growth of white spruce at the tree line in Arctic Alaska. (**A**) Map of Northern Alaska showing tree line (green), October sea ice extent, and study watersheds. Field, field sites; RS, remotely sensed sites. Transects are yellow and weather stations are indicated by red triangles. (**B**) Spearman correlations (ρ) of 1980-2018 individual tree ring width index series (RWI series) (n = 1,636 trees) with 1979–2017 October open water area time series (OWA series, blue) and 1980–2018 June mean air temperature series (Jun T, red) by watersheds. Solid-colored circles represent significant ($P \leq 0.05$) correlations and translucent symbols represent those that are nonsignificant. The OWA series was assembled from OWA = $(d_B\ \mathrm{OWA}_{\mathrm{Chukchi}} + d_C\ \mathrm{OWA}_{\mathrm{Beaufort}})/(d_B + d_C)$, where d_B and d_C give location-to-coastline distances for Beaufort and Chukchi coastlines, respectively. (**C**) Correlation of the RWI series with the OWA series versus correlation of the RWI series with Jun T. Each circle represents an individual tree. Rug plots indicate marginal distributions. Dotted line gives equality with ρ OWA > ρ Jun T above the line. Color gives significance as indicated in legend. (**D**) Density ridgeplots of the RWI series correlations with the OWA series (upper) and Jun T (lower) by lifetime growth rate quartile. Lifetime mean diameter growth rates were estimated from 4124 crossdated tree ring measurement series with pith offset estimates.

values of the OWA series, $\overline{OWA}$, and OWA trend are associated with proximity to the Chukchi's increasing and historically greater October open water area.

Measuring tree line responses to sea ice area and its loss

The OWA series provided an opportunity to measure the correlation between adult radial tree growth and sea ice retreat. We detrended tree ring width (RWI) series and extracted auto-regressive residuals (AR series) of 1636 individual white spruce trees (*47*), then correlated the tree ring series with OWA series and several growing season air temperature series (fig. S2). Because white spruce growth can have time lags with air temperature (*4*), temperature series included gridded annual time series of the current and previous year growing season as individual monthly means (June, July, and August), and as means of monthly sequences (June–July, July–August, and June–July–August). OWA and temperature series were prewhitened for investigating their correlations with AR series.

We explored the spatial gradient of $\overline{OWA}$ as a predictor of several environmental covariates of spruce performance metrics sampled at the individual tree or plot level (*47*). During 2019 we sampled adult lateral branch foliar concentrations of nitrogen (N, percent), $\delta^{15}N$ (per mil), and phosphorous (P, percent) as proxies for soil nutrient availability, and carbon $\delta^{13}C$ and soil moisture (percent) as proxies for water availability. We recorded 2019-2022 temperatures (temperatures) of air (AirT at 2 m) and soil (SoilT at −10 cm) with dataloggers and estimated mean snowpack depth in January (ø Jan snowpack, cm) using a geophysical model (fig. S3) parameterized with a six-year Brooks Range snow-fence experiment (fig. S4). Performance metrics included 2019 adult lateral branch extension (adult growth, millimeters); 2015-2020 relative growth rate of seedlings (height < 0.5 m) (seedling growth, y^{-1}); and sapling (0.5 ≤ height <1.4 m) density (saplings, m^{-2}) measured once during 2019 to 2022. We grouped samples by tree line and aggregated each variable with its mean. Using tree line means as observations in linear mixed-effects models (with random factor watershed to address spatial autocorrelation), we quantified the responses of environmental covariates to $\overline{OWA}$ as a predictor variable, and of white spruce performance metrics to the environmental covariates.

The OWA trend mostly covered the interval of repeat imagery that we used to determine rates of elevation gain by forests (forest advance) (*47*). Within 50 km^2 sample areas, we matched orthophotos from 1970 to 1982 with satellite scenes from 2009 to 2020 (*47*). Using flexible binomial generalized additive models (GAMs), we calculated the mean elevation difference between equal probabilities of spruce presence during historical and recent periods. Dividing mean elevation differences by time between image captures estimated rates (meters per decade). To confirm these estimates, we sampled ~2500 km of field transects along and across tree lines (Fig. 1A) where we located >2000 spruce colonists <2.5 m tall and >500 m beyond the tree line. We binned colonist and nearest tree line elevations into 0.5° longitudinal bands, found bin-wise maximum elevations of colonists and tree lines, then differenced them as $\overline{\Delta E}$ (meters). We then compared forest advance with PRISM precipitation.

We tested hypothetical pathways between temporally static $\overline{OWA}$ and white spruce performance metrics and between temporal OWA trend and forest advance through piecewise structural equation modeling (pSEMs) (*47*). In pSEMs, variables can act as responses and predictors simultaneously in a set of linear mixed-effects models whose graphical representation is a network of potential causal pathways.

Tree ring growth responds more to sea ice retreat than to growing season temperatures

The tree ring RWI series correlated more strongly with the OWA series ($\bar{\rho}$ = 0.23) than with current June air temperature, the temperature series with the highest count of significant correlations ($\bar{\rho}$ = 0.17) (Fig. 1, B and C, and fig. S5, A and B). One-third of RWI and AR correlations with the OWA series were significant versus one-fifth of June correlations. Across the Brooks Range, fast-growing individuals generally showed stronger correlations than did slow-growing individuals (Fig. 1D and figs. S5 to S7). However, the AR series correlations revealed a significant interaction between growth and longitude, with fast-growing trees in the colder east responding more positively to interannual variation in the OWA series than fast-growing trees in the warmer west (fig. S7). Because young, fast-growing trees are responsible for ecotone advance and eastern trees respond more sensitively to OWA series than western ones, temporal change in Arctic Ocean conditions appears to play a role in boreal forest advance. However, less than half of the trees showed significant correlations, thus suggesting that other factors are also important to tree growth and ecotone advance.

Life-stage performance metrics differ in their responses to covariates at the tree line

Using the datalogger temperatures, we found that overall mean January–March (winter) temperatures increased with $\overline{OWA}$ more so than did mean June–August (summer) temperatures (fig. S8). The modeled ø Jan snowpack also increased monotonically with $\overline{OWA}$ SoilT correlated more positively with the ø Jan snowpack (r = 0.75, fig. S9) than with winter AirT (r = 0.56), consistent with snow's insulative value (*35*, *48*). In turn, life stage–specific performance metrics were greater where temperatures, snowpack, and nutrient availability were greater (fig. 2). By contrast, adult (Fig. 2, K to O) and seedling growth (Fig. 2, A to E) (together growth) showed significant positive responses to annual and winter temperatures and ø Jan snowpack. Seedling growth, consistent with seedling sensitivity to winter conditions (*2*, *16*, *23*, *39*, *40*), increased more strongly with winter temperatures than did adult growth. Saplings (Fig. 2, F to J) contrasted with growth through a nonsignificant response to ø Jan snowpack and significant positive response to soil moisture. Growth also showed significant responses to nutrient availability (Fig. 2, P to T).

Forest advance shows a threshold response to snowpack depth

Investigation of repeat imagery separated by four decades revealed that in more maritime watersheds ($\overline{OWA} > \overline{OWA}$), mean upslope forest advance modeled by binomial GAMs (6.6 ± 1.4 m $decade^{-1}$, n = 13 watersheds) was nearly twice that found in more continental watersheds ($\overline{OWA} < \overline{OWA}$) (3.4 ± 0.6, n = 9). Similarly, along field transects the mean elevation of colonists above established tree lines in more maritime watersheds ($\overline{\Delta E}$ ± se = 197 ± 36, n = 13 bins) was 1.7 times that of colonists in more continental watersheds (118 ± 31, n = 7). When compared with monthly PRISM precipitation variables singularly and in sequence, forest advance responded more strongly to subfreezing months ($\overline{SoilT}$ < 0°C) than to above-freezing ones (Fig. 3A). Importantly, forest advance demonstrated a threshold response to snowpack depth. A segmented linear regression against PRISM Jan snowpack revealed a breakpoint at 44.8 ± 2.0 cm. Above this, forest advance responded positively and strongly to greater snowpack depth (Fig. 3C). In 5 of those 12 watersheds where PRISM Jan snowpack was shallower than 45 cm, forest advance was less than spatial errors inherent in the remote sensing (*47*). These results support studies suggesting that shallow snowpacks prevent seedling recruitment to saplings (*2*, *9*, *16*, *22*, *23*, *35–40*), thereby slowing ecotone advance.

Open Arctic Ocean water leads to improved growth, recruitment, and range expansion through pathways that involve snowpack and soil properties

Comparing piecewise structural equation modeling (pSEMs) between performance metrics and forest advance indicated that qualitatively similar pathways lead from OWA-based exogenous variables to terminal nodes (Fig. 4). For example, positive pathways lead through snowpack or soil temperatures to growth and forest advance, highlighting the importance of snow in facilitating ecotone advance (*2*, *9*, *16*, *22*, *23*, *35–40*).

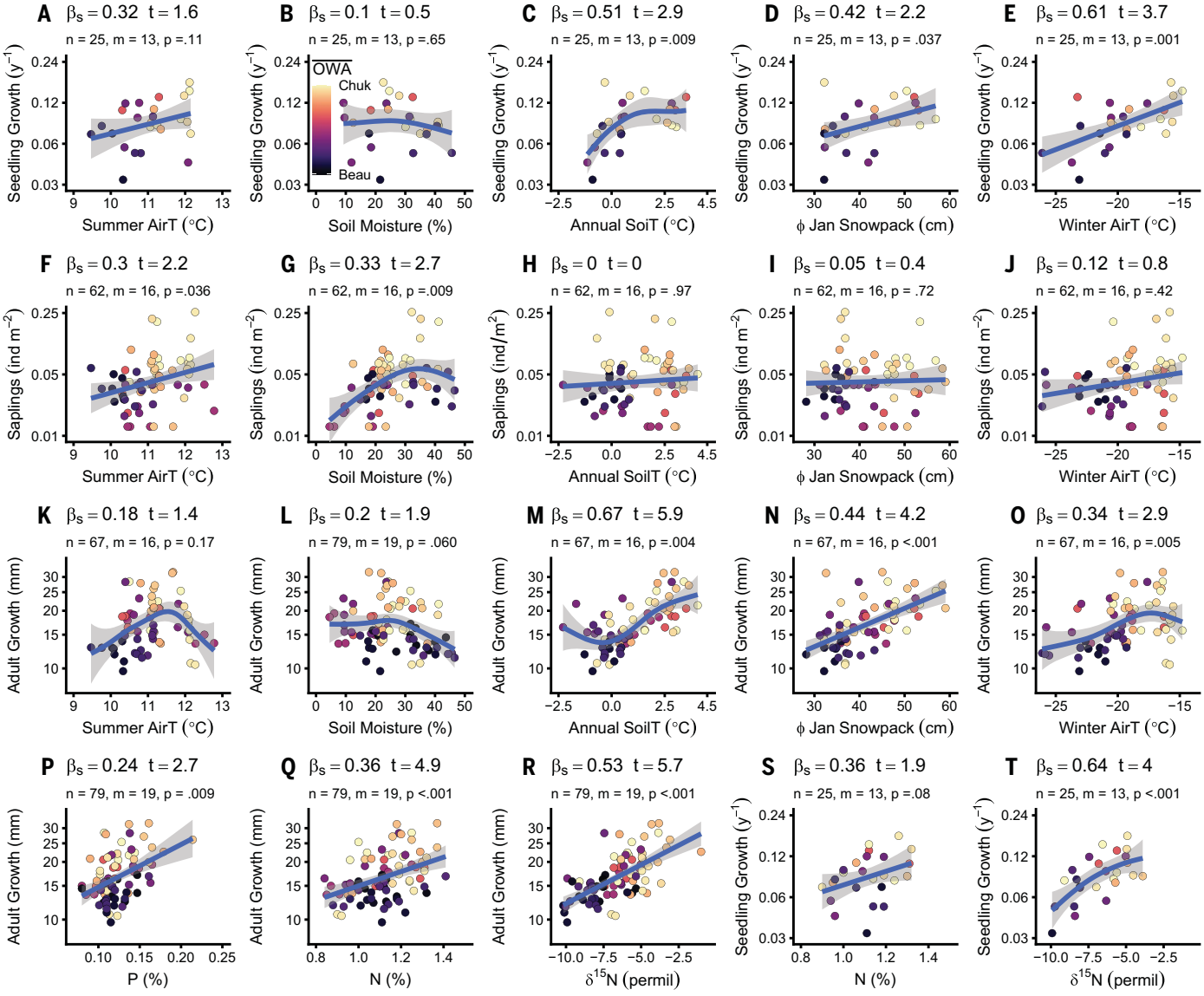

Fig. 2. White spruce response to environmental covariates associated with sea ice retreat. (**A** to **E**) Response of seedling terminal leader relative growth rate (seedling growth), (**F** to **J**) sapling density (saplings), and (**K** to **O**) adult lateral branch growth (adult growth) to environmental covariates (from left to right) June-August (summer) air temperature (AirT), soil moisture, annual soil temperature (SoilT), January snowpack depth from geophysical model (ø Jan snowpack), and Nov-Mar (winter) AirT. (**P** to **T**) Last row shows response of adult (left three panels) and seedling growth (right two panels) to foliar nutrient means of adult samples from tree lines. In each panel, $ß_s$ indicates standardized coefficient; t, Wald-test; p, p-value for covariate from linear mixed-effects model with Watershed as random factor. n, number of tree lines (observations); m, number of watershed study sites (random factor levels). Given the distance-weighted-average time series of Chukchi and Beaufort October open water as the OWA series, the overall mean of OWA series ($\overline{OWA}$) for each watershed is static. Colors indicate $\overline{OWA}$ with $\overline{OWA} > \overline{\overline{OWA}}$ more maritime (orange and yellowish hues) and $\overline{OWA} < \overline{\overline{OWA}}$ more continental (darker hues). Spruce metrics on log scale. Values are means of tree lines for one-time measurements and 3-year overall means for AirT and SoilT and ø Jan snowpack.

Adult growth and forest advance pathways also connected soil temperature to N, a known limiting nutrient (*36–39*). Forest advance and sapling pSEMs shared negative pathways that included air temperature (*9*), which when combined with the positive sapling pathway involving soil moisture implies that moisture limitation (*4*) of sapling recruitment slows ecotone advance. The sapling pSEM differed most from other pSEMs. Its direct negative snowpack effect suggests the possibility of a nonlinear ecotone response to snow. We speculate that because of their intermediate size, saplings may suffer both from pathogenic snow fungi that inhabit snowpacks (*40*) and from reduced cambial activity in deeper, longer lasting snowpacks (*49*). The direct positive $\overline{OWA}$ pathway to saplings represents an unidentified mechanism related to sea ice loss.

In summary, the differing pathways among life stages support the idea of multiple bottlenecks (*2–5, 8–40*), but their overall similarities emphasize that OWA, winter conditions, and soil properties modulate ecotone advance. The pSEMs lack evidence for direct positive effects of air temperature. Because young trees are most relevant for ecotone advance, their stronger response to OWA shown here, and in the tree ring width response shown above, support an Arctic Ocean tree line relationship that may apply more broadly.

Proportionally more circumarctic tree lines advance where proximal to ongoing sea ice loss

In a meta-analysis combining our 22 forest advance rates with 60 other circumarctic sites

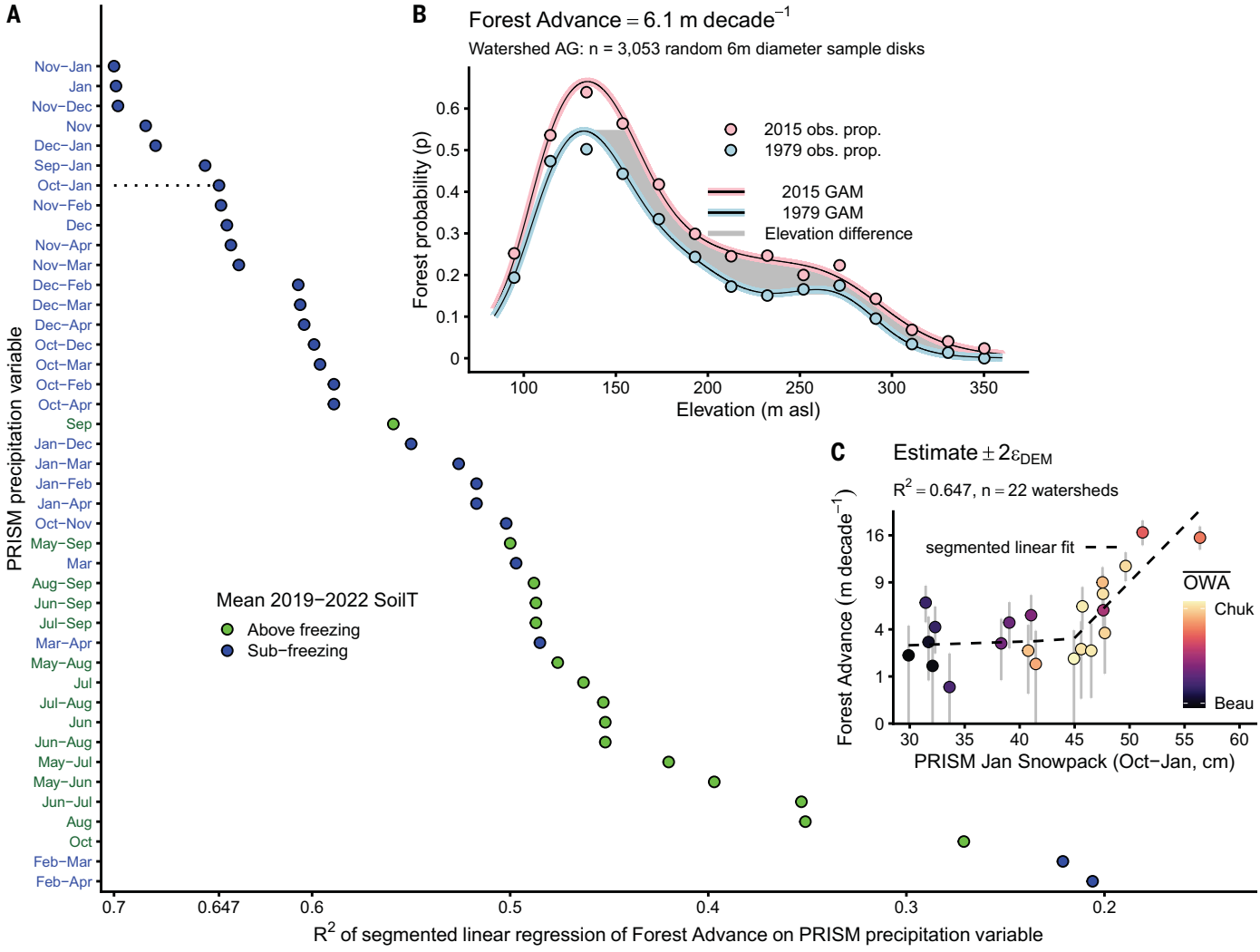

Fig. 3. Response of forest advance to winter precipitation. (**A**) Precipitation variables ranked by R^2 from segmented regression of forest advance on mean precipitation variables extracted from PRISM at remotely-sensed watershed sample sites (Fig. 1A). Blue text and blue circles indicate mean SoilT < 0°C, and green text and green circles ≥ 0°C. SoilT: 2019-2022 average of n = 315 dataloggers (10 cm below ground) at m = 69 tree lines among w = 16 watersheds. (**B**) Example of historical (1979, blue) and recent (2015, pink) forest probability as function of elevation using a binomial generalized additive model fit to raw presence/absence data at watershed "AG" in Fig. 1A. Gray polygon is dense set of segments connecting equal probabilities (Δp = 0.001) between GAMs. Segment mean divided by 3.6 decades gives 6.1 m decade^{-1}. Observed proportions of forest (filled circles) in elevation bins illustrate fits. (**C**) Plot and segmented regression of forest advance on precipitation variable October-January as horizontal dotted line in (A). The temporally static $\overline{OWA}$ for each watershed is the overall mean of the OWA series, the latter defined as distance-weighted-average time series of Chukchi and Beaufort October open water. Colors indicate $\overline{OWA}$, with $\overline{OWA} > \overline{\overline{OWA}}$ as more maritime and $\overline{OWA} < \overline{\overline{OWA}}$ as more continental. Vertical axis is nonlinear. ε DEM = SD (error) of ArcticDEM.

previously published (Fig. 5A), we contested six generalized linear mixed-effects models of ecotone advance as a binary response to four predictors. Predictors included latitude and historical 1979 sea ice cover, historical 1979 OWA, and 1979–2009 OWA-trend of the Arctic Ocean sea nearest to each site. The best-performing model indicated that ecotone advance has occurred more often where open water area has increased rapidly over time or sea ice cover was historically limited. In particular, Chukchi and Kara Sea open water gains increased the odds of advance at nearby ecotones, whereas persistent Beaufort and East Siberian ice reduced the odds. Historically low OWA in Hudson Bay and the Barents Sea left odds of nearby ecotone advance even. These results offer a climatic mechanism underpinning correlations of ecotone advance with winter precipitation (*9*).

Discussion and outlook

Circumarctic patterns, pSEMs, forest advance–snowpack relationships, and tree ring responses to the OWA series make a compelling case for sea ice retreat and absence as ultimate causal factors prompting boreal forest advance. Consistent with previous observations of growth and recruitment at ecotones (*2, 14–16, 18–26, 30–40*), the spatially extensive results shown here confirm that warmer temperatures and deeper snowpacks can drive forest advance through increased growth and survival of individual trees and that growth stages differ in their responses to environmental covariates. The multiple stages through which individual trees pass from seeds to adults introduce nonlinearity and time lags to forest advance, in part because of the interplay between plant height and microclimate (*2*, *26*, *40*). Nevertheless, we have demonstrated that an opening Arctic Ocean associated with global and regional

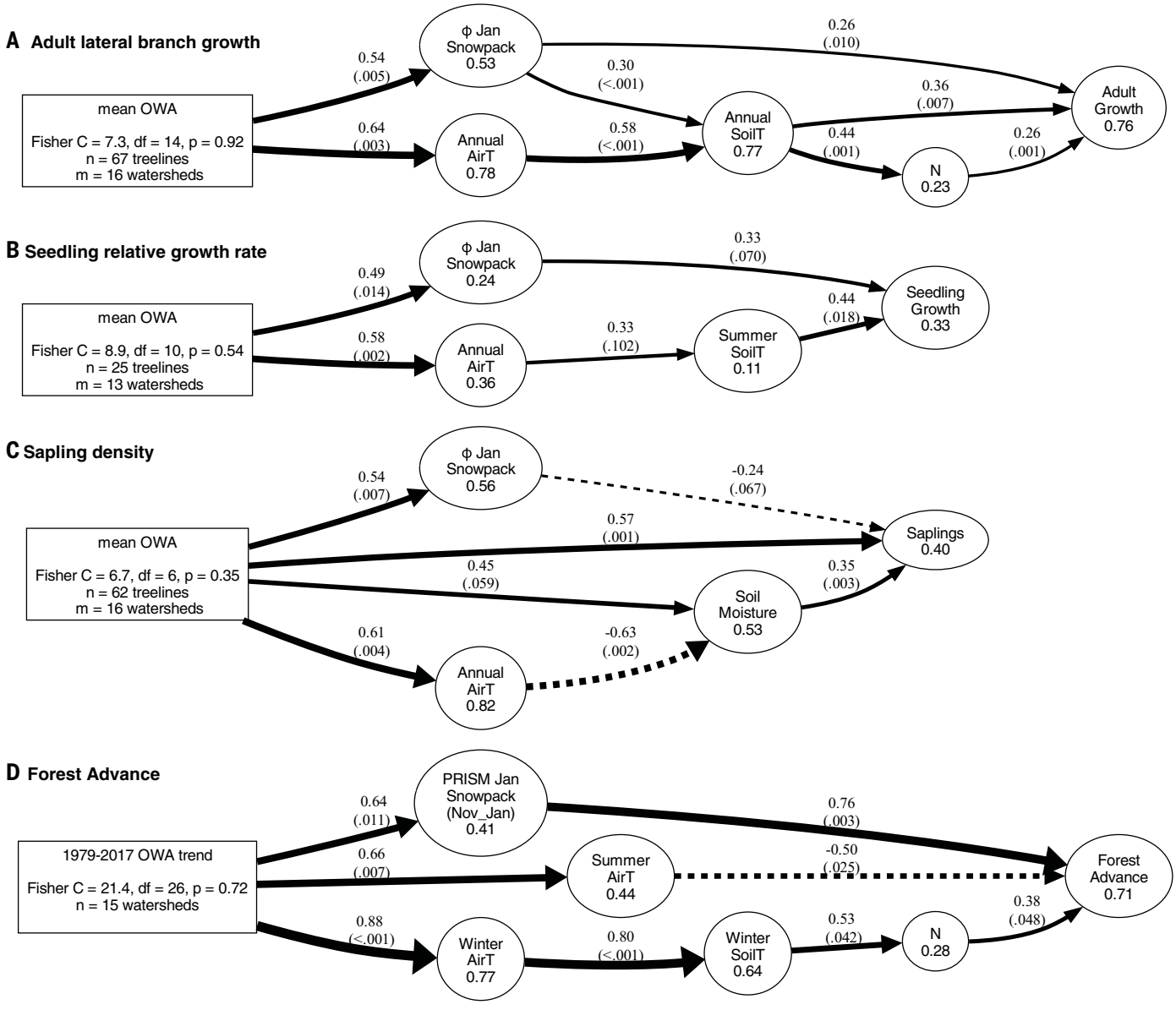

Fig. 4. Piecewise structural equation models (pSEMs) linking the distance weighted 1979-2017 October open water area time series to spruce performance metrics as overall mean *OWA* and to forest advance as temporal trend (OWA trend). (**A**) Adult lateral branch extension (adult growth), (**B**) seedling relative growth (seedling growth), (**C**) Sapling density (saplings), and (**D**) forest advance. Exogeneous variable *OWA* is defined as mean 1979-2017 exposure to October to open water in Chukchi and Beaufort Seas weighted by distance (OWA series). Exogeneous variable OWA-trend defined as Theil-Sen regression slope of the OWA series during 1979 to 2017. Statistics in exogenous variable boxes give C, Fisher's C statistic for pSEM; p, probability that C is greater than df in support of each pSEM; n, tree lines included; m, watersheds included. Numbers below endogenous variable names give conditional, fixed factor R^2. Numbers along arrows give standardized coefficients from pSEMs with *P*-values in parentheses. Solid arrows indicate positive effects; dashed arrows indicate negative effects. Arrow widths are proportional to standardized coefficients.

climates favors tree growth and establishment, fueling the replacement of arctic tundra by boreal forest.

Warming associated with influx of latent heat and inflow of Atlantic Ocean water will continue to erode Arctic sea ice proximal to western Siberia (*43*). Meanwhile, the combined extent of the Beaufort Gyre's multiyear ice (*41*) and the Queen Elizabeth Archipelago will maintain continental conditions across northwestern Canada (*10*). These contrasting dynamics suggest that ecotones in western Siberia will be the next to advance whereas those in northern Canada will likely remain stagnant the longest (*10–12*, *14*, *15*, *32*). Near the Barents Sea (*17*, *18*, *20*) and Hudson Bay (*2*, *13*, *20*, *21*, *23*), autumn ice was mostly absent throughout the 19th and 20th centuries (*44*), leaving open water effects complete. Now other factors may limit the ecotones there, particularly water stress, fire (*2–5*), edaphic conditions, and topography (*10–12*) near Hudson Bay, in addition to herbivory (*18*, *21*) and land use (*2*, *26*) near the Barents Sea.

Recursive warming and reduced habitat for tundra organisms due to boreal forest advance will critically affect resource availability for Arctic-dwelling people (*6*, *7*). However, even with rapid boreal forest expansion, it is unlikely that northward advance (*9*, *16*, *50*)

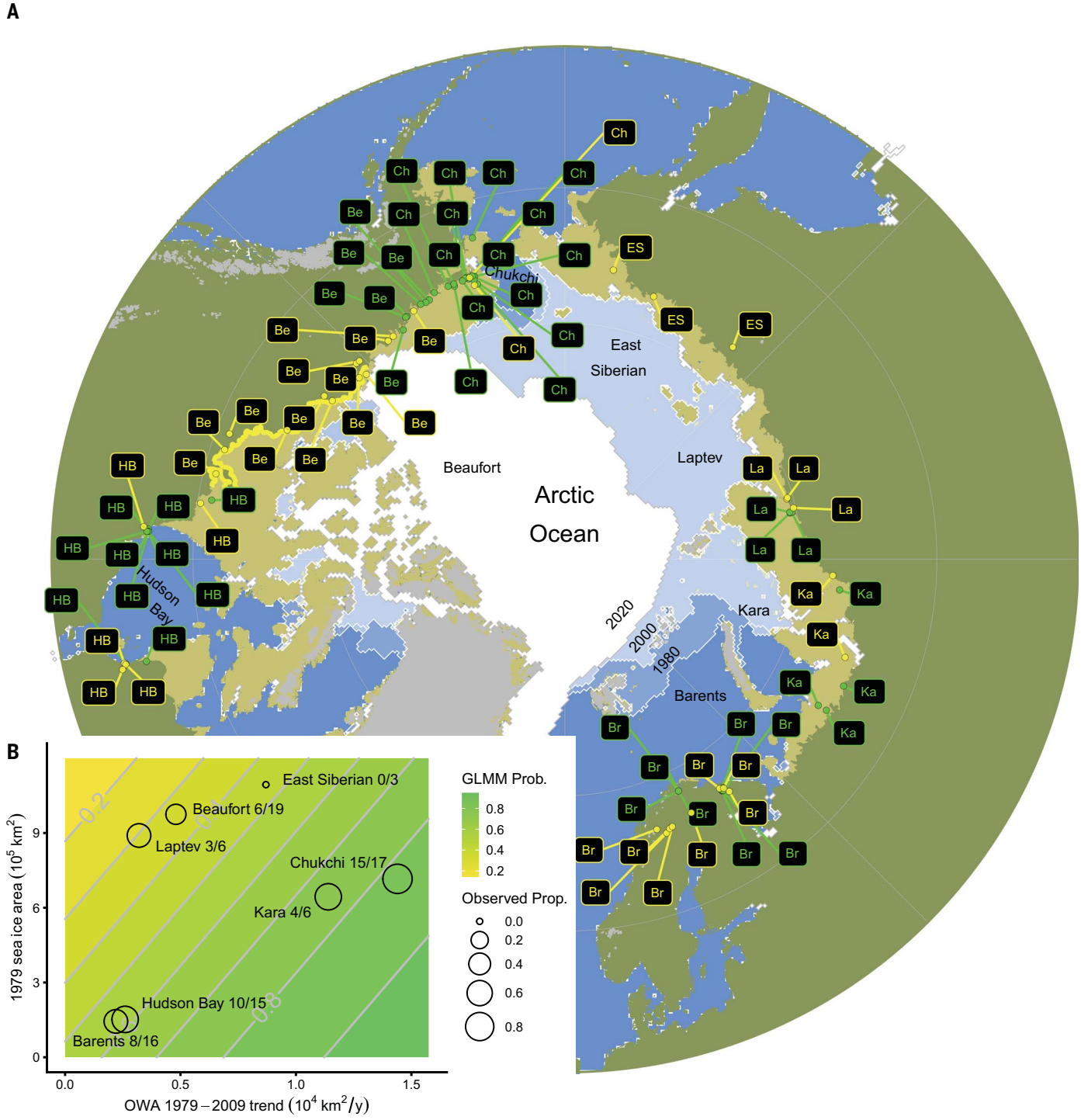

Fig. 5. Circumarctic ecotone advance, sea ice, and open ocean water trend. (**A**) Colored dots give locations of ecotones advancing (green) and not-advancing (yellow) with two-letter code labels indicating nearest Arctic Ocean sea: Br, Barents; Ka, Kara; La, Laptev; ES, East Siberia; Ch, Chukchi; Be, Beaufort; HB, Hudson Bay. October sea ice extent in 2020, 2000, and 1980 is indicated by a white polygon bounded by a gray line, a white polygon bounded by a gray line, and a light blue polygon bounded by a white line, respectively. Blue areas indicates open water in 1980; gray, glaciers; tan, Arctic vegetation; olive green, non-Arctic vegetation. (**B**) Observations of proportions (circles) and graphical portrayal of predicted probability of ecotone advance (0 = bright yellow, 1 = dark green) from generalized linear mixed-effects binomial model (random factor with k = 10 spatial groups). Predictor variables include the 1979–2009 October open water trend (OWA-trend) on the *x*-axis and 1979 sea ice area on the *y*-axis. Observed proportions labeled proximal sea with integers giving advancing over total number of ecotones.

will outpace southern forest retreat (*51*) in the face of current climate change and other anthropogenic forcings. Although the causes of boreal forest expansion across the Arctic can be anticipated, the full consequences of this and other biome shifts remain unknown.

REFERENCES AND NOTES

1. C. Körner, E. Spehn, *Science* **365**, 1061–1061 (2019).
2. S. Payette, C. Lavoie, *Environ. Rev.* **2**, 78–90 (1994).
3. G. M. MacDonald, J. M. Szeicz, J. Claricoates, K. A. Dale, *Ann. Assoc. Am. Geogr.* **88**, 183–208 (1998).
4. M. Wilmking, G. P. Juday, *Global Planet. Change* **47**, 282–300 (2005).
5. G. M. MacDonald, K. V. Kremenetski, D. W. Beilman, *Philos. Trans. R. Soc. B* **363**, 2285–2299 (2008).
6. J. Settele *et al*., in *Terrestrial and Inland Water Systems* (Cambridge University Press, 2014), pp. 271–360.
7. F. S. Chapin 3rd *et al*., *Science* **310**, 657–660 (2005).
8. G. V. Frost, H. E. Epstein, *Glob. Change Biol.* **20**, 1264–1277 (2014).
9. W. G. Rees *et al*., *Glob. Change Biol.* **26**, 3965–3977 (2020).
10. K. P. Timoney *et al*., *Ecoscience* **26**, 133–148 (2019).
11. K. P. Timoney, *Ecoscience* **30**, 113–129 (2023).
12. K. P. Timoney, S. Mamet, *Ecoscience* **27**, 93–106 (2020).
13. S. D. Mamet, G. P. Kershaw, *J. Biogeogr.* **39**, 855–868 (2012).
14. H. Z. Travers-Smith, T. C. Lantz, *Ecosphere* **11**, e03118 (2020).
15. T. C. Lantz, N. D. Moffat, R. H. Fraser, X. Walker, *Arct. Sci.* **5**, 167–184 (2019).
16. R. J. Dial, C. T. Maher, R. E. Hewitt, P. F. Sullivan, *Nature* **608**, 546–551 (2022).
17. A. Hofgaard *et al*., *Ecosystems* **22**, 434–451 (2019).
18. A. Hofgaard, L. Dalen, H. Hytteborn, *J. Veg. Sci.* **20**, 1133–1144 (2009).
19. D. Kambo, R. K. Danby, *J. Plant Ecol.* **11**, 411–422 (2018).
20. C. D. Brown *et al*., *Ecography* **42**, 137–147 (2019).
21. L. Brehaut *et al*., *J. Biogeogr.* **50**, 476–488 (2023).
22. B. Sveinbjörnsson, A. Hofgaard, A. Lloyd, *Ambio* **12**, 23–29 (2002).
23. S. M. Renard, E. J. B. McIntire, A. Fajardo, *J. Veg. Sci.* **27**, 29–39 (2016).
24. K. D. Dearborn, R. K. Danby, *Clim. Change* **150**, 211–225 (2018).
25. D. Kambo, R. K. Danby, *Ecosphere* **9**, e02176 (2018).
26. F. Holtmeier, G. Broll, *Glob. Ecol. Biogeogr.* **14**, 395–410 (2005).
27. I. Shevtsova *et al*., *Environ. Res. Lett.* **15**, 085006 (2020).
28. M. Wieczorek *et al*., *Ecology* **98**, 2343–2355 (2017).
29. S. Kruse *et al*., *Biogeosciences* **16**, 1211–1224 (2019).
30. C. Körner, *Trends Ecol. Evol.* **36**, 979–989 (2021).
31. C. A. Roland, J. H. Schmidt, J. F. Johnstone, *Oecologia* **174**, 665–677 (2014).
32. X. Walker, G. H. R. Henry, K. McLeod, A. Hofgaard, *Glob. Change Biol.* **18**, 3202–3211 (2012).
33. K. Okano, M. S. Bret-Harte, *SpringerPlus* **4**, 79 (2015).
34. S. E. Hobbie, F. S. ChapinIII, *J. Ecol.* **86**, 449–461 (2002).
35. P. F. Sullivan, *Biogeochemistry* **99**, 65–77 (2010).
36. P. F. Sullivan, S. B. Ellison, R. W. McNown, A. H. Brownlee, B. Sveinbjörnsson, *Ecology* **96**, 716–727 (2015).
37. S. B. Z. Ellison, P. F. Sullivan, S. M. P. Cahoon, R. E. Hewitt, *Ecology* **100**, e02878 (2019).
38. R. W. McNown, P. F. Sullivan, *Funct. Ecol.* **27**, 672–683 (2013).
39. R. K. Danby, D. S. Hik, *Glob. Change Biol.* **13**, 437–451 (2007).
40. I. Barbeito, M. A. Dawes, C. Rixen, J. Senn, P. Bebi, *Ecology* **93**, 389–401 (2012).
41. T. Vihma *et al*., *J. Geophys. Res. Biogeosci.* **121**, 586–620 (2016).
42. V. L. Ford, O. W. Frauenfeld, *Global Planet. Change* **209**, 103752 (2022).
43. L. N. Boisvert *et al*., *J. Clim.* **31**, 8441–8462 (2018).
44. J. E. Walsh, F. Fetterer, J. Scott Stewart, W. L. Chapman, *Geogr. Rev.* **107**, 89–107 (2019).
45. J. E. Walsh, W. L. Chapman, F. Fetterer, S. Stewart, Gridded monthly sea ice extent and concentration, 1850 onward, Version 2, National Snow and Ice Data Center (2019); https://doi.org/10.7265/jj4s-tq79.
46. PRISM Climate Group, Oregon State University, Northwest Alliance for Computational Science & Engineering, PRISM Alaska gridded monthly precipitation, (2018); https://prism.oregonstate.edu/projects/alaska.php.
47. Materials and methods are available as supplementary materials.
48. B. Taras, M. Sturm, G. E. Liston, *J. Hydrometeorol.* **3**, 377–394 (2002).
49. E. A. Vaganov, M. K. Hughes, A. V. Kirdyanov, F. H. Schweingruber, P. P. Silkin, *Nature* **400**, 149–151 (1999).
50. L. T. Berner, S. J. Goetz, *Glob. Change Biol.* **28**, 3275–3292 (2022).
51. R. Rotbarth *et al*., *Nat. Commun.* **14**, 3373 (2023).

ACKNOWLEDGMENTS

P. Adkins, L. Berner, P. Burns, D. Cooper, A. Dahl, G. Dana, P. Dial, J. Ditto, S. Donahue, J. Geck, N. Hooper, N. Blankenship, D. Louangaphay, A. Ethington, R. Koleser, J. Cramer, V. Lytle, T. Matsuoka, F. McCarthy, B. Meiklejohn, F. Restrepo, S. Ryan, S. Smeltz, S. Taylor, B. Weissenbach, K. Vicich, and D. Wright assisted with remote sensing, GIS, field, and/or lab assistance. J. Cummings, D. Nickisch, E. Sieh, and K. Sweetsir provided air transport. Alpacka Raft and Hyperlite Mountain Gear provided in-kind expedition equipment. We appreciate the efforts of the three anonymous reviewers. USNPS permitted the research as NOAT-2021-SCI-0002, GAAR-2021-SCI-0004, and GAAR-2019-SCI-0002 and USNFWS as ANWR 2019-S4.
Funding: This work was supported by the following: National Science Foundation 1504538, 1748849, 2133494 (to P.F.S.); National Science Foundation Office of Polar Programs 1748847 (to R.E.H.); National Science Foundation Office of Polar Programs 1748773, Alaska National Aeronautics and Space Administration EPSCoR, and Explorers Club/Discovery Grant (to R.J.D.); National Aeronautics and Space Administration through the Alaska Space Grant Program (to R.E.W., R.J.D., and his students) Shoreline, Incorporated (to R.J.D.) National Institute of General Medical Sciences of the National Institutes of Health under 1UL1GM118991 (to R.J.D.). The work is solely the responsibility of the authors and does not necessarily represent the official view of the National Institutes of Health.
Author contributions: Conceptualization: R.J.D., P.F.S., C.T.M., and R.E.W. Methodology: R.J.D., P.F.S., C.T.M., A.M.W., R.E.W., M.G.Z., D.J.C., and R.E.H. Investigation: R.J.D., P.F.S., C.T.M., R.E.H., A.M.W., R.E.W., M.G.Z., and D.J.C. Field logistics: P.F.S., R.J.D., C.T.M., R.E.W., and M.G.Z. Fieldwork: R.E.W., R.J.D., C.T.M., M.G.Z., P.F.S., A.M.W., and R.E.H. Dendrochronology: C.T.M., D.J.C., M.G.Z., and P.F.S. Visualization: R.J.D., P.F.S., C.T.M., A.M.W., R.E.W., R.E.H., and D.J.C. Formal Analysis: R.J.D., C.T.M., A.M.W., P.F.S., and R.E.W. Funding acquisition: R.J.D., P.F.S., R.E.H., and R.E.W. Project administration: P.F.S., R.J.D., and R.E.H. Data curation: R.J.D., P.F.S., C.T.M., A.M.W., R.E.W., M.G.Z., and D.J.C. Supervision: R.J.D., P.F.S., C.T.M., A.M.W., R.E.W., D.J.C., and R.E.H. Writing – original draft: R.J.D., C.T.M., P.F.S., and A.M.W. Writing – review and editing: R.J.D., P.F.S., C.T.M., R.E.H., A.M.W., R.E.W., D.J.C., and M.G.Z.
Competing interests: Authors declare that they have no competing interests. **Data and materials availability:** All data, code, and materials used for analysis (*52–61*) are available at the National Science Foundation's Arctic Data Center or are available on-line as cited in the Materials and Methods section of the Supplementary Materials.

SUPPLEMENTARY MATERIALS

science.org/doi/10.1126/science.adh2339
Materials and Methods
Supplementary Text
Figs. S1 to S9
References (*52–110*)
MDAR Reproducibility Checklist

Submitted 22 February 2023; accepted 12 January 2024
10.1126/science.adh2339